

## Simultaneously rapid synthesis and consolidation of nanostructured Ti-TiC composites from TiH<sub>2</sub> and CNT by high-frequency induction heating and their mechanical properties

In-Jin Shon<sup>a,\*</sup>, Byung-Su Kim<sup>b</sup>, Jin-Kook Yoon<sup>c</sup>, Kyung-Tae Hong<sup>c</sup> and Na-Ra Park<sup>a</sup>

<sup>a</sup>Division of Advanced Materials Engineering, the Research Center of Hydrogen and Fuel Cell, Chonbuk National University, 664-14 Deokjin-dong 1-ga, Deokjin-gu, Jeonju, Jeonbuk 561-756, Korea

<sup>b</sup>Minerals Resources Research Division, Korea Institute of Geoscience and Mineral Resources, Daejeon, 305-350 Korea

<sup>c</sup>Materials Architecturing Research Center, Korea Institute of Science and Technology, PO Box 131, Cheongryang, Seoul 130-650, Korea

TiH<sub>2</sub> and CNT powders were milled by high energy ball milling. The milled powders were then simultaneously synthesized and consolidated using high frequency induction heated sintering (HFIHS) within one minute under the applied pressure of 80 MPa. The advantage of this process is not only rapid densification to near theoretical density but also to prevent grain growth in nano-structured materials. The milling did not induce any reaction between the constituent powders. Meanwhile, HFIHS of the TiH<sub>2</sub>-CNT mixture produced a Ti-TiC composite according to the reaction  $(0.92\text{TiH}_2 + 0.08\text{CNT} \rightarrow 0.92\text{Ti} + 0.08\text{TiC} + 0.92\text{H}_2)$ ,  $(0.84\text{TiH}_2 + 0.16\text{CNT} \rightarrow 0.84\text{Ti} + 0.16\text{TiC} + 0.84\text{H}_2)$ . Highly dense nanocrystalline Ti-TiC composites with a relative density of up to 99.8% were obtained within one minute. The hardness and fracture toughness of the dense Ti-8 mole% TiC and Ti-16 mole% TiC produced by HFIHS were also investigated. Not only fracture toughness and but also hardness values of Ti-16 mole% TiC composite were higher than those of Ti-8 mole% TiC composite.

**Key words:** Rapid sintering, Composite, Nanomaterials, Mechanical Properties, Ti-TiC.

### Introduction

Metal-ceramic composites have been developed to find the optimum combination of low density, high oxidation resistance and high hardness of ceramic and metal toughness. They are recommended as candidates for bio-materials, aerospace, automotive and defense applications.

Ti has a density of 4.506 g cm<sup>-3</sup>, a Young's modulus of 116 GPa, a biocompatibility and good fracture toughness. The attractive properties of titanium carbide is high hardness, low density, relatively high thermal and electrical conductivities. TiC is also very stable, with a melting temperature of 2727 K, and does not undergo phase transformations. Hence, a microstructure consisting of Ti and TiC may be able to satisfy the mechanical property requirements of structural materials.

Nanocrystalline materials can be obtained with improved physical and mechanical properties [1, 2]. Nanomaterials have received attention for their high strength, high hardness, excellent ductility and toughness [3, 4]. Recently, nanocrystalline powders have been produced by high-energy milling [5, 6]. The sintering

temperature of high-energy mechanically milled powder is lower than that of unmilled powder due to the increased reactivity, internal and surface energies, and surface area of the milled powder, contributing to its so-called mechanical activation [7-9]. The grain size in sintered materials becomes much larger than that in pre-sintered powders due to rapid grain growth during a conventional sintering process. Therefore, controlling grain growth during sintering is one of the keys to the commercial success of nanostructured materials. A high frequency induction heated sintering method wherein the densification is completed within 5 minutes has shown to be very successful in controlling grain growth during the sintering process [10-12]. The HFIHS also takes advantage of simultaneously applying mechanical pressure and induced current during sintering. As a result, the sintering temperature is expected to decrease because applying mechanical pressure affects the driving force of the sintering.

This paper reports on the simultaneously rapid synthesis and consolidation of dense nanostructured Ti-TiC composites starting with high-energy ball-milled TiH<sub>2</sub> and CNT nanopowders. The mechanical properties and grain sizes of the resulting nanostructured Ti-TiC composite were also evaluated.

### Experimental Procedures

TiH<sub>2</sub> (99.5%, -200 mesh, Sejong) and CNT (Carbon

\*Corresponding author:  
Tel : +82-63-270-2381  
Fax: +82-63-270-2386  
E-mail: ijshon@chonbuk.ac.kr

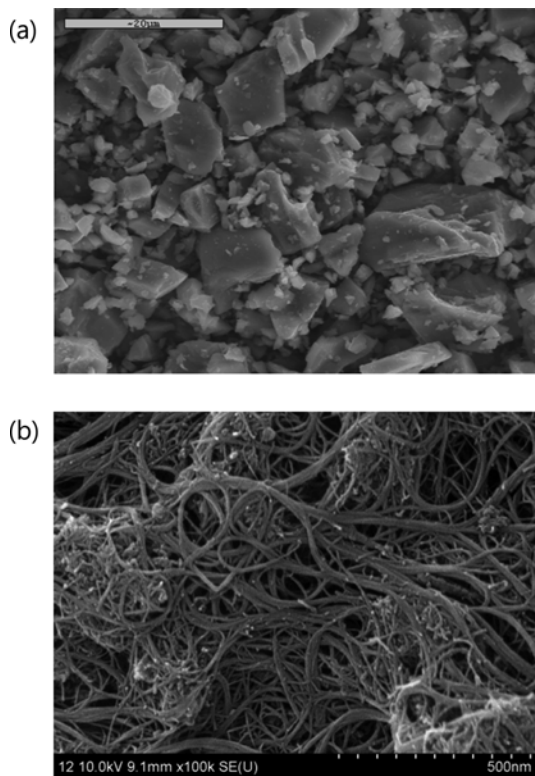


Fig. 1. SEM images of raw materials : (a) TiH<sub>2</sub>, (b) CNT.

Nanotechnologies Incorporated) powders were used as raw materials. The TiH<sub>2</sub> and CNT powders are shown in Fig. 1. TiH<sub>2</sub> and CNT powders were mixed in a high energy ball mill. For high-energy ball milling, a Pulverisette-5 planetary mill was used at 250 rpm for 10 h. Tungsten carbide balls (8.5 mm in diameter) were used for milling in a sealed cylindrical stainless steel vial under argon atmosphere. The weight ratio of ball-to-powder was 30 : 1. After the milling process, the grain sizes of the mixed TiH<sub>2</sub> and CNT powders were calculated by Suryanarayana and Norton's formula [13]:

$$B_r(B_{\text{crystalline}} + B_{\text{strain}})\cos\theta = k \lambda/L + \eta\sin\theta \quad (1)$$

where  $B_r$  is the full width at half-maximum (FWHM) of the diffraction peak after instrumental correction,  $B_{\text{crystalline}}$  and  $B_{\text{strain}}$  are FWHM caused by the small grain size and internal stress, respectively,  $k$  is a constant (with a value of 0.9),  $\lambda$  is the wavelength of the X-ray radiation;  $L$  and  $\eta$  are the grain size and internal strain, respectively; and  $\theta$  is the Bragg angle. The parameters  $B$  and  $B_r$  follow Cauchy's form with the relationship:  $B = B_r + B_s$ , where  $B$  and  $B_s$  are the FWHM of the broadened Bragg peak and the standard sample's Bragg peaks, respectively.

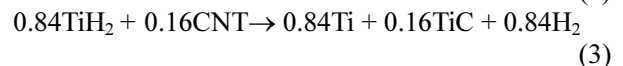
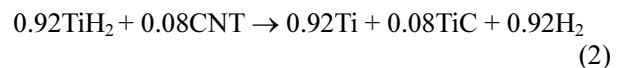
After the milling processes, the milled powders were placed in a graphite die (outside diameter, 35 mm; inside diameter, 10 mm; height, 40 mm) and were then introduced into the high frequency induction heated

sintering system (Eltek, South Korea), shown schematically in Ref. [10-12]. The four major stages in the sintering process were as follows: Stage 1 involved the creation of a vacuum in the system. During Stage 2, a uniaxial pressure of 80 MPa was applied. During Stage 3, an induced current flowed into the system and was maintained at 1170 °C with a heating rate of 1200 °C/min. The system was then turned off without a holding time. A pyrometer focused on the surface of the graphite die measured the temperature during HFIHS. Finally, during Stage 4, the sample was cooled to room temperature. The process was carried out under a vacuum of 5.33 Pa.

The relative densities of the sintered sample were measured by the Archimedes method. Microstructural information was obtained from polished Ti-TiC composites. Compositional and microstructural analyses of the products were performed using X-ray diffraction (XRD), and scanning electron microscopy (SEM) with energy dispersive X-ray analysis (EDAX). Vickers hardness was measured by performing indentations at load of 10 kg and a dwell time of 15 s on the sintered samples.

## Results and Discussion

The interaction between TiH<sub>2</sub> and CNT, i.e.,



are thermodynamically feasible above 800K as shown in Fig. 2.

Figure 3 shows x-ray diffraction patterns of high energy ball milled powders. Only TiH<sub>2</sub> peaks were identified after milling. This indicates that reaction (2) and (3) did not occur during the high energy ball milling method. However, the full width at half-maximum (FWHM) of the diffraction peak in Fig. 3(a) and (b) are broad due to the refinement of powders and strains. Therefore, powder milled using the high energy ball milling method was smaller than that of raw powder. SEM images of TiH<sub>2</sub>-8 mole% CNT and TiH<sub>2</sub>-16 mole% CNT milled for 10h are shown in Fig. 4(a) and (b), respectively. TiH<sub>2</sub> powders were very fine and CNT distributed uniformly.

The shrinkage displacement-time (temperature) curve provides useful information on the consolidation behavior. Fig. 5 shows the shrinkage record of TiH<sub>2</sub>-8 mole % CNT, and TiH<sub>2</sub>-16 mole % CNT compacts. In all cases, the shrinkage displacements are nearly constant up to 550 °C at which point they abruptly increase above that temperature. Afterwards, they contract almost linearly above temperature of 950 °C at which the consolidation terminates. The shrinkage curve suggests

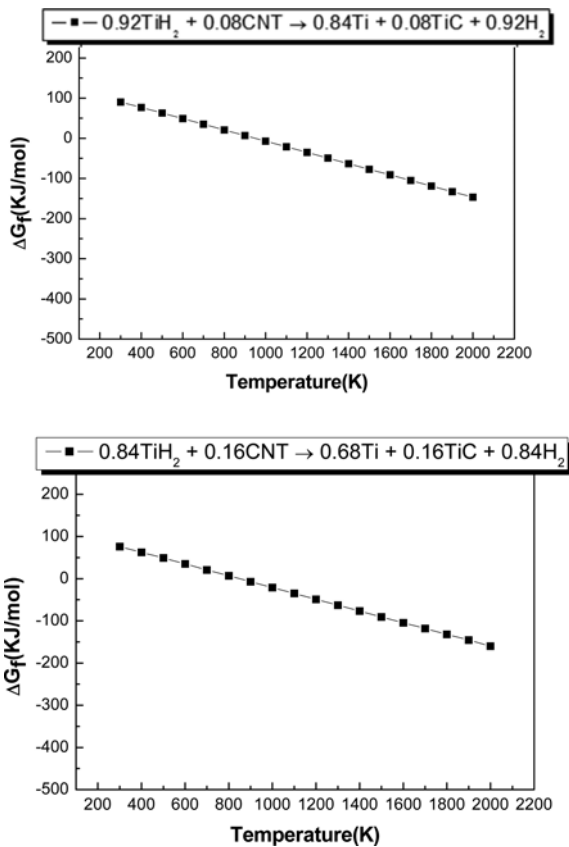


Fig. 2. Temperature dependence of the Gibbs free energy variation by interaction of  $TiH_2$  with CNT.

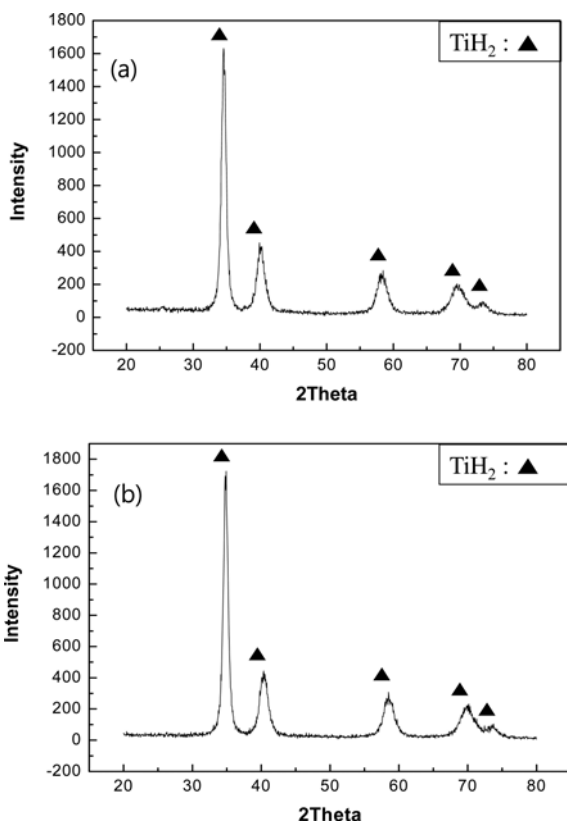


Fig. 3. XRD patterns of mechanically milled powders: (a)  $TiH_2$ -8 mole% CNT, (b)  $TiH_2$ -16 mole% CNT.

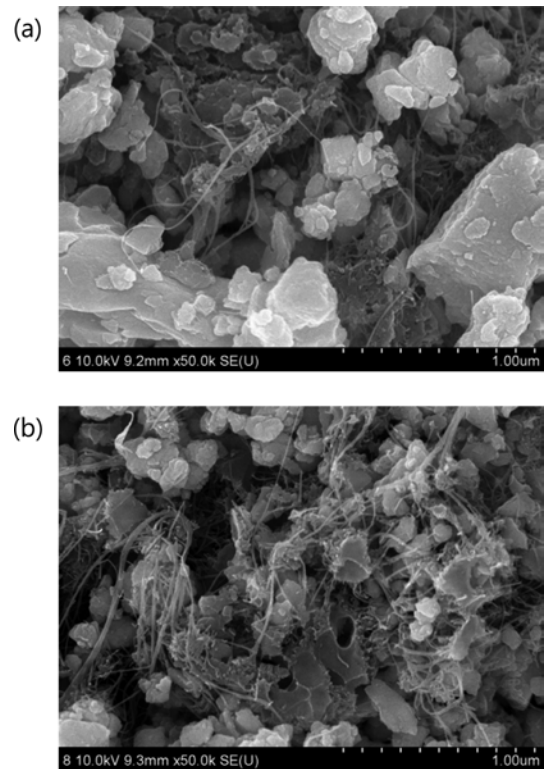


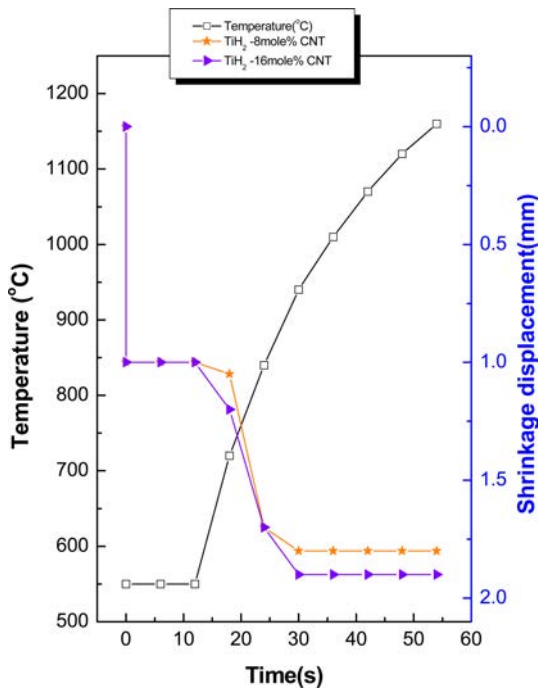
Fig. 4. SEM images of mechanically milled powders: (a)  $TiH_2$ -8 mole% CNT, (b)  $TiH_2$ -16 mole% CNT.

that the consolidation terminates in one minute.

These powders were rapidly sintered under the application of high pressure (80 MPa) which had a significant effect on the total driving force,  $F_D$ , defined as [14]

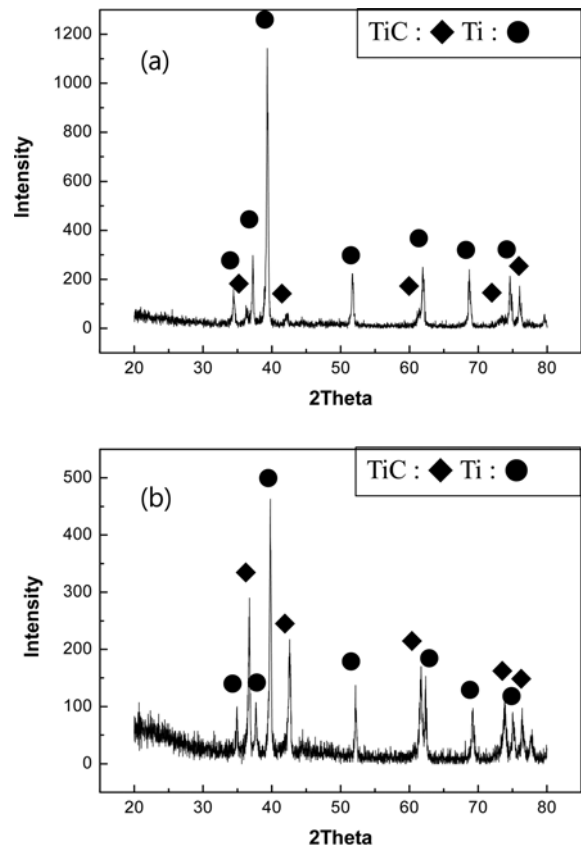
$$F_D = \gamma + (P_a r / \pi), \quad (4)$$

where  $g$  is the surface energy,  $P_a$  is the applied pressure, and  $r$  is the radius of the particle. The effect of pressure on the densification of  $TiO_2$  during high-frequency induction heated sintering was investigated by Shon *et al.* [15]. A significant increase in the relative density was observed as the pressure increased from about 60 to 100 MPa during sintering at 800 °C. Secondly, the role of the current (resistive or inductive) in sintering and or synthesis has been the focus of several attempts aimed at providing an explanation for the observed enhancement of sintering and the improved characteristics of the products. The role played by the current has been interpreted in various ways, the effect being explained in terms of the fast heating rate due to Joule heating, the presence of plasma in pores separating powder particles, and the intrinsic contribution of the current to mass transport [16-19]. Thirdly, raw powders were very fine and many defects were introduced by high-energy ball milling. So, The powders were activated, and contact points for diffusion route increased.



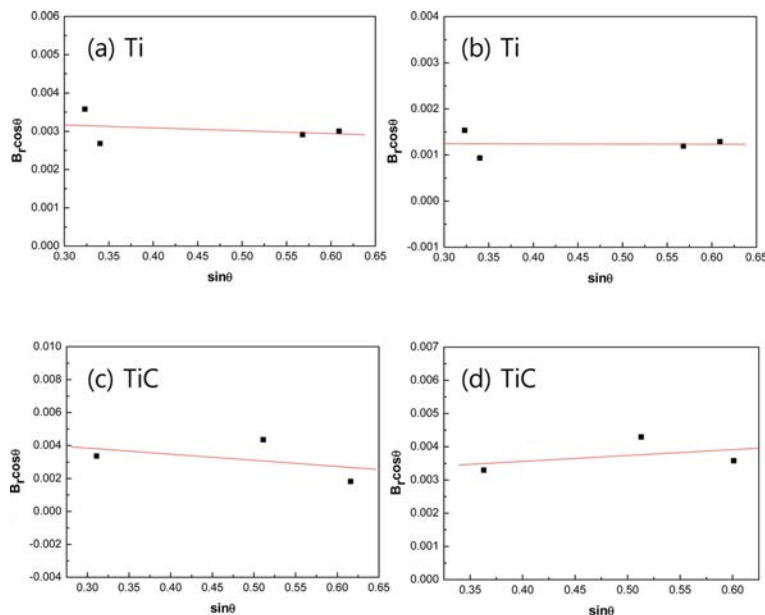
**Fig. 5.** Variations of temperature and shrinkage displacement with heating time during the sintering of TiH<sub>2</sub>-8 mole% CNT, and TiH<sub>2</sub>-16 mole% CNT by HFIHS.

Figure 6 shows XRD patterns of the high-energy ball milled powder heated to 1170 °C in which only Ti and TiC peaks are detected. Figure 7 indicates plot of  $B_r \cos \theta$  versus  $\sin \theta$  to calculate the grain size of Ti and TiC in Ti-8 mole % TiC and TiC-16 mole % TiC composites, respectively. The average grain sizes of Ti and TiC in the composites sintered from high energy ball milled powders are 103 nm, 41 nm and 28 nm, 49 nm which were obtained from X-ray data in Fig. 6



**Fig. 6.** XRD patterns of (a) Ti-8.7 mole% TiC and (b) Ti-19 mole% TiC composites sintered from high energy ball milled powders.

by Suryanarayana and Norton's formulas. Figure 8 shows the SEM images and X-ray mappings of Ti-8 mole % TiC, and Ti-16 mole % TiC samples heated to 1170 °C. Nearly full dense Ti-8 mole % TiC, and Ti-



**Fig. 7.** Plot of  $B_r \cos \theta$  versus  $\sin \theta$  of Ti and TiC in Ti-8.7 mole% TiC and Ti-19 mole% TiC composites, respectively.

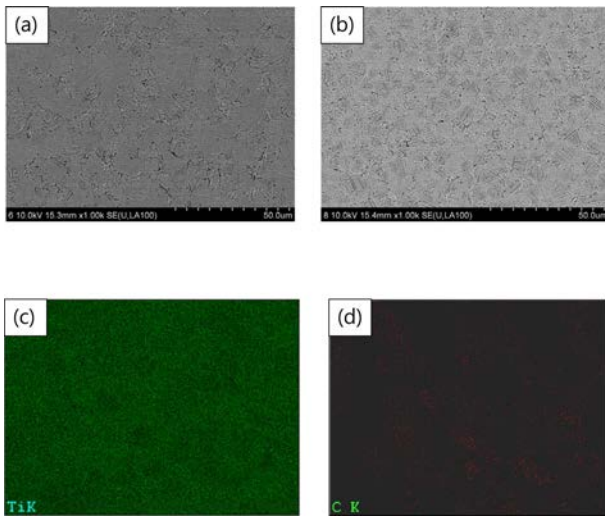


**Fig. 8.** SEM images and X-ray mapping of Ti-TiC system : (a) Ti-8.7 mole% TiC and (b) Ti-19 mole% TiC (c) Ti mapping and (d) C mapping.

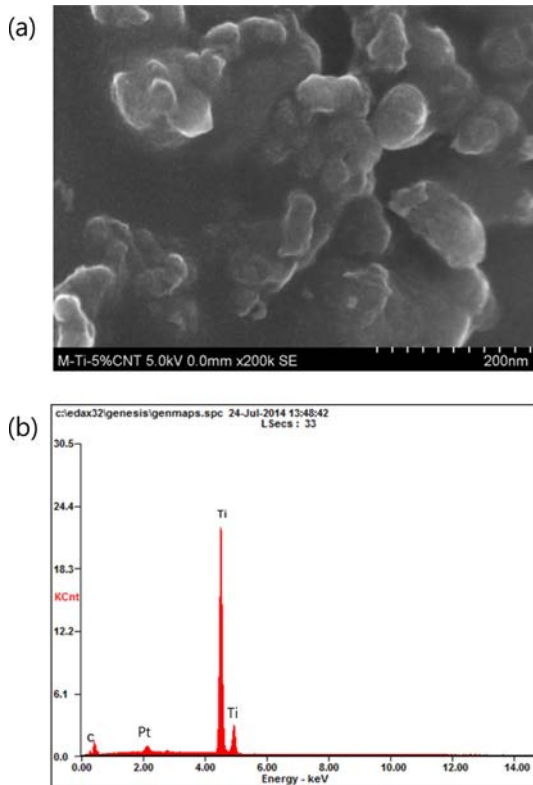


**Fig. 9.** FE-SEM image and EDS of a Ti-16 mole% TiC composite.

16 mole % TiC composites were observed in Fig. 8(a) and (b). The corresponding relative density were 99.7 and 99.8%. In X-ray mappings, Ti was detected in all areas in Fig. 8(c) and C was uniformly distributed according to position in Fig. 8(d). From the X-ray mapping, TiC was homogeneously imbedded in Ti. FE-SEM image and EDS of Ti-16 mole % TiC composite was shown in Figure 9. It is also obvious that the microstructure consists of nanograins in Fig. 9(a). In EDS, Ti, C and Pt peaks were detected. Pt comes from

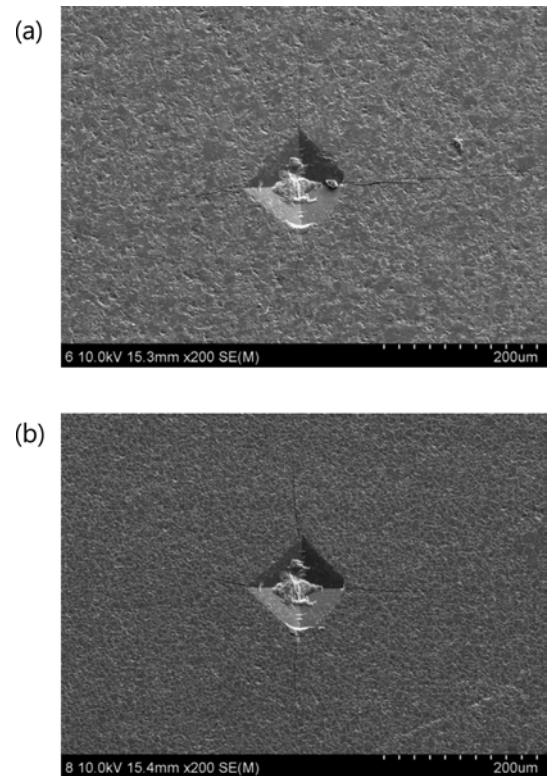


**Fig. 10.** Vickers hardness indentation in (a) Ti-8.7 mole% TiC and (b) Ti-19 mole% TiC composites.

surface coating that enables clear observation of the microstructure. And there are no other peaks, such as Fe or W, which can possibly happen during the milling process.

Vickers hardness measurements were made on polished sections of the Ti-8 mole % TiC and TiC-16 mole % TiC composites composite using a 10 kg<sub>f</sub> load and a 15 s dwell time. The calculated hardness value of Ti-8 mole % TiC and TiC-16 mole.% TiC composites sintered at 1170 °C from high energy ball milled powders were 875 and 980 kg/mm<sup>2</sup>, respectively. These values represent an average of five measurements. Indentations with large enough loads produced median cracks around the indentation. The length of these cracks permits an estimation of the fracture toughness of the material. From the length of these cracks, fracture toughness values can be determined using the equation by Anstis *et al.* [20]

$$K_{IC} = 0.016(E/H)^{1/2} \cdot P/C^{3/2} \quad (5)$$

where E is Young's modulus, H the indentation hardness, P the indentation load, and C the trace length of the crack measured from the center of the indentation. The modulus was estimated by the rule of mixtures for the 0.09 and 0.18 volume fraction of TiC and the 0.91 and 0.82 volume fraction of Ti in Ti-8 mole % TiC and TiC-16 mole.% TiC composites, using E(TiC) = 517.9 GPa [21] and E(Ti) = 116 GPa [22]. As in the case of hardness

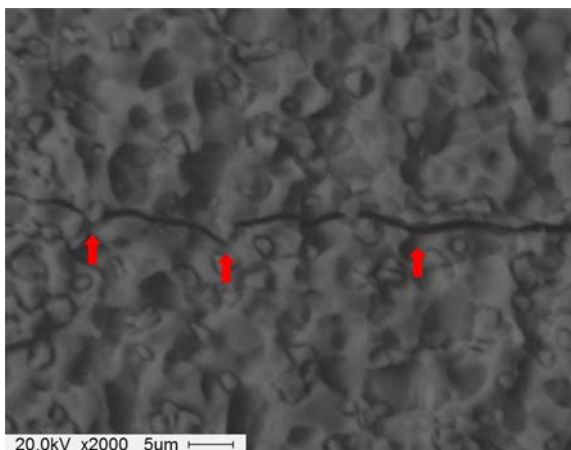


Fig. 11. Crack propagation in a Ti-16 mole% TiC composite.

values, the toughness values were derived from the average of five measurements. The toughness values of Ti-8 mole% TiC and TiC-16 mole% TiC composites obtained from high energy ball milled powders are 5.9 and 7.8 MPa · m<sup>1/2</sup>, respectively.

Kim *et al.* [23] studied the sintering of nanostructured Ti from milled TiH<sub>2</sub> by high-frequency induction heating. The hardness of nanostructured Ti was reported as 567 kg/mm<sup>2</sup>. The hardness values of Ti-8mole% TiC and TiC-16mole% TiC composites were higher than that of TiC due to addition of TiC hard phase as expected. Comparing hardness and fracture toughness of Ti-8 mole% TiC with TiC-16 mole% TiC, both hardness and fracture toughness increased simultaneously with an increase in TiC content. Figure 10 shows Vickers indentation in the Ti-8 mole% TiC and TiC-16 mole% TiC composites sintered from high energy ball milled powders. One to three additional cracks were propagated from the indentation corner. The toughness of Ti-TiC composites may be that the TiC may deter the crack propagation. Fig. 11 shows a crack propagated in a deflective manner (↑) in TiC-16mole% TiC composite. It is believed that the enhanced fracture toughness of TiC-16 mole% TiC is a result of TiC in the composite, deterring crack propagation.

## Conclusions

TiH<sub>2</sub> nanopowders were made by a high energy ball milling method. Using high-frequency induction heated sintering, simultaneous synthesis and densification of Ti-8mole% TiC with Ti-16mole% TiC composites was accomplished. Relative densities of the sintered specimens were 99.7% and 99.8%, respectively. The average grain sizes of Ti and TiC in the composites sintered from high energy ball milled powders are 103 nm, 41 nm and 28 nm, 49 nm. The calculated hardness value of Ti-8 mole % TiC and TiC-16 mole.% TiC composites were 875, 980 kg/

mm<sup>2</sup> and 5.9, 7.8 MPa · m<sup>1/2</sup>, respectively. The hardness and fracture toughness of the TiC-16 mole% TiC composite are higher than those of Ti-8 mole% TiC composite. It is believed that the enhanced hardness and fracture toughness of TiC-16 mole% TiC composite is a result of the addition of hard TiC and TiC in the composite, may deterring crack propagation.

## Acknowledgments

This work was supported by the KIST Institutional Program (Project No. 2E25374-15-096) and was supported by a grant in aid awarded by the Basic Research Project of the Korea Institute of Geoscience and Mineral Resources (KIGAM), funded by the Ministry of Science, ICT and Future Planning (GP20 15036).

## References

1. El-Eskandarany MS. *J Alloys Compd* 305 (2000) 225-38.
2. Fu L, Cao LH, Fan YS. *Scr Mater* 44 (2001)1061-8.
3. S. Ni. Y.B. Wang, X.Z. Liao, S.N. Alhajeri, H.Q. Li, Y.H. Zhao, E.J. Lavernia, S.P. Ringer, T.G. Langdon, Y.T. Zhu, *Materials Science and Engineering A* 528 (2011) 3398-3403.
4. Berger S, Porat R, Rosen R. *Prog Mater Sci* 42 (1997) 311-20.
5. G.W. Lee, I.J. Shon, *Korean J. Met. Mater.* 51 (2013) 95-100.
6. I.J. Shon, G.W. Lee, J.M. Doh, J.K. Yoon, *Electronic Materials Letters*, 9 (2013) 219-225.
7. F. Charlot, E. Gaffet, B. Zeghmati, F. Bernard, J. C. Liepce, *Mater. Sci. Eng. A262*, (1999) 279-278.
8. Hyun-Su Kang, Jung-Mann Doh, Jin-Kook Yoon, and In-Jin Shon, *Korean J. Met. Mater.* 52 (2014) 759-764.
9. M.K. Beyer, H. Clausen-Schaumann, *Chem. Rev.* 105, (2005) 2921-2948.
10. Na-Ra Park, Kwon-Il Na, Hanjung Kwon, Jae-Won Lim, and In-Jin Shon, *Korean J. Met. Mater.* 51 (2013) 753-759.
11. Song-Lee Du, Jung-Mann Doh, Jin-Kook Yoon, and In-Jin Shon, *Korean J. Met. Mater.* 51 (2013) 579-584.
12. I.J. Shon, *Korean J. Met. Mater.* 52 (2014) 573-580.
13. Suryanarayana C, Grant Norton M. *X-ray diffraction a practical approach*. New York: Plenum Press; 1998. p. 213.
14. Coble R. L. *J Appl Phys* 41 (1970) 4798-807.
15. Kim HC, Park HK, Shon IJ, Ko IY. *Journal of Ceramic Processing Research* 7 (2006) 327-31.
16. Shen Z, Johnsson M, Zhao Z, Nygren M. *J Am Ceram Soc* 85 (2002) 1921-7.
17. Garay JE, Anselmi-Tamburini U, Munir ZA, Glade SC, Asoka-Kumar P. *Appl Phys Lett* 85 (2004) 573-5.
18. Friedman JR, Garay JE, Anselmi-Tamburini U, Munir ZA. *Intermetallics* 12 (2004) 589-97.
19. Garay JE, Garay JE, Anselmi-Tamburini U, Munir ZA. *Acta Mater* 51 (2003) 4487-95.
20. Anstis GR, Chantikul P, Lawn BR, Marshall DB. *J Am Ceram Soc* 64 (1981) 533-8.
21. Jiwoong Kim, Shinhoo Kang, *Journal of Alloys and Compounds* 528 (2012) 20-27.
22. [http://en.wikipedia.org/wiki/Elastic\\_properties\\_of\\_the\\_elements](http://en.wikipedia.org/wiki/Elastic_properties_of_the_elements) (data page).
23. Na-Ri Kim, Sung-Wook Cho, Won-Baek Kim and In-Jin Shon, *Korean J. Met. Mater.*, Vol. 50, No. 1(2012) pp. 34-38.